GEOPHYSICS, VOL. 80, NO. 3 (MAY-JUNE 2015); P. D195–D206, 9 FIGS., 4 TABLES.
10.1190/GEO2014-0167.1

Nuclear magnetic resonance average pore-size estimations outside the fast-diffusion regime

Mike Müller-Petke[1], Raphael Dlugosch[1], Jochen Lehmann-Horn[2], and Mathias Ronczka[1]

ABSTRACT

The pore-size distribution (PSD) of geologic materials is an important rock parameter to understand the flow of water in the subsurface. PSDs can be obtained from sieving analyses, mercury porosimetry measurements, and imaging techniques, but none of these methods is available for in situ measurements. Nuclear magnetic resonance (NMR) measurements are controlled by rock parameters such as the surface-area to pore-volume ratio. NMR is available for in situ measurements. State-of-the-art NMR relaxation time measurements need a calibration of the surface relaxivity ρ to extract pore-size information. State-of-the-art NMR diffusion measurements avoid the calibration of ρ but are limited to small pores. We developed an approach that estimates the average pore size without calibrating ρ by means of incorporating higher order modes into the signal interpretation of NMR relaxation times. We conducted forward-modeling studies using an analytic solution for cylindrical tubes, 2D finite-element simulations to incorporate fractal pore spaces, and laboratory experiments on synthetic and natural samples. Our experimental data indicated that relaxation can occur outside the fast-diffusion regime not only for coarse-grained materials, but also for fine- to medium-grained unconsolidated sandy materials due to high surface relaxivities. We found that the rock-fluid interface's roughness had a significant impact on the diffusion regime and led to an apparent increase in ρ, which may cause intermediate or slow diffusion. The methodology was limited to materials with a narrow PSD and uniform distribution of ρ because we assumed multiexponential decay due to diffusion in single isolated pores.

INTRODUCTION

Knowledge of the subsurface's hydraulic conductivity distribution K is a key to predict the flow of water through shallow aquifers and porous media. Estimates of K are obtained using various permeameter realizations or analyses of pore sizes (Butler, 2005). Carrier (2003) gives handy formulas based on the work of Kozeny (1927) and Carman (1939), reducing the particle-size distribution to an effective hydraulic pore radius to estimate K, whereas Brooks and Corey (1964) incorporate the complete pore-size distribution (PSD) into their analyses. Common approaches to determine PSDs use imaging techniques (Straley et al., 1987) or mercury porosimetry (Brakel et al., 1981). Alternatively, the pore surface area of a sample can be measured by the Brunauer-Emmet-Teller (BET) approach to estimate an average pore radius (Keating and Knight, 2010). These techniques are not available for measurements from the earth's surface or during logging. In in situ studies, K can be estimated using aquifer and slug tests. Multilevel slug tests, dipole-flow tests, and borehole-flowmeter tests provide K as a function of depth. These techniques suffer from limited depth resolution, long screening intervals, long measurement times, and considerable complexity in the data analysis and uncertainties (Butler, 2005).

Nuclear magnetic resonance (NMR) is a versatile tool in the physical sciences, and it is well known for its imaging and spectroscopy applications in medicine, chemistry, and the geosciences (Callaghan, 2007). NMR instruments are available for laboratory (Fukushima and Roeder, 1981), borehole (Dunn et al., 2002), and surface-based (Dlugosch et al., 2011) geophysical applications. Its sensitivity to ^{1}H makes it an attractive method to determine the water content of porous materials, and pore-size information can be extracted by transforming the NMR quantities of relaxation time or pore fluid self-diffusion. The transformation process from NMR

Manuscript received by the Editor 11 April 2014; revised manuscript received 17 November 2014; published online 18 March 2015.
[1]Leibniz Institute for Applied Geophysics, Hannover, Germany. E-mail: mike.mueller-petke@liag-hannover.de; raphael.dlugosch@liag-hannover.de; mathias.ronczka@liag-hannover.de.
[2]CSIRO Process Science and Engineering, Lucas Heights, New South Wales, Australia. E-mail: jochen.lehmann-horn@csiro.au.

quantities to pore-size information depends on a priori knowledge, namely, assumptions on the material's specific parameters and the diffusion regime (Figure 1).

Relaxation in the fast-diffusion regime occurs when (1) the volume within the pore space covered by the Brownian motion during relaxation is at least several times larger than the pore size (Brownstein and Tarr, 1979) and (2) a moderately homogeneous surface relaxivity ρ throughout the pore space (Keating and Knight, 2012) can be assumed. In the fast-diffusion regime, a broad or multimodal distribution of relaxation times (RTD), i.e., a multiexponential decay, translates to a broad or multimodal PSD, and a monoexponential signal translates to a narrow PSD or a single (average) pore size (see Figure 1). In conventional relaxation time experiments, calibrating ρ is necessary to transfer RTD to PSD or directly to K (Kenyon et al., 1988) because otherwise, RTDs only indicate a certain relative distribution of pore sizes but do not represent true PSDs. An ideal field practice for calibration is to extract a representative sample, conduct laboratory measurements, and apply the obtained calibration for the complete log (e.g., Coates et al., 1999). More recently, Dlubac et al. (2013) compare different calibration methods, including laboratory measurements of samples, logging data from pressure tools, and wellbore flow. Parsekian et al. (2014) present results using the above-mentioned common hydrologic techniques, such as the multilevel slug test and a statistical approach, to obtain calibration parameters for borehole applications. Outside the fast-diffusion regime, commonly referred to as the slow- and intermediate-diffusion regimes, the situation becomes more complicated; RTDs may not translate into PSDs because multiexponential decays can be observed from a single pore size due to higher order relaxation modes (Brownstein and Tarr, 1979). Moreover, Keating and Falzone (2013) report difficulties developing a calibration method to recover pore sizes from NMR RTDs.

To avoid calibration, pulsed-field-gradient (PFG) measurements to determine the pore fluid self-diffusion coefficient (Stejskal and Tanner, 1965) have been shown to provide an estimate of the average pore radius (Mitra et al., 1993; Hürlimann et al., 1994; Vogt et al., 2002; Pape et al., 2006). Probing restricted diffusion using PFG sequences is limited to cases in which the pore geometry has an effect on the self-diffusion coefficient; i.e., the root-mean-square displacement of a proton in the free fluid is larger than the average pore size (Stallmach and Kärger, 1999). PFG-based pore-size estimations can therefore be used when relaxation occurs in small pores (mostly the fast-diffusion regime) but cannot provide information on large pores (mostly outside the fast-diffusion regime). The technique has been extended to fixed-field gradients (FFGs) because PFG sequences are not available in many in situ logging tools (Hürlimann and Grin, 2000; Hürlimann and Venkataramanan, 2002; Hürlimann et al., 2002).

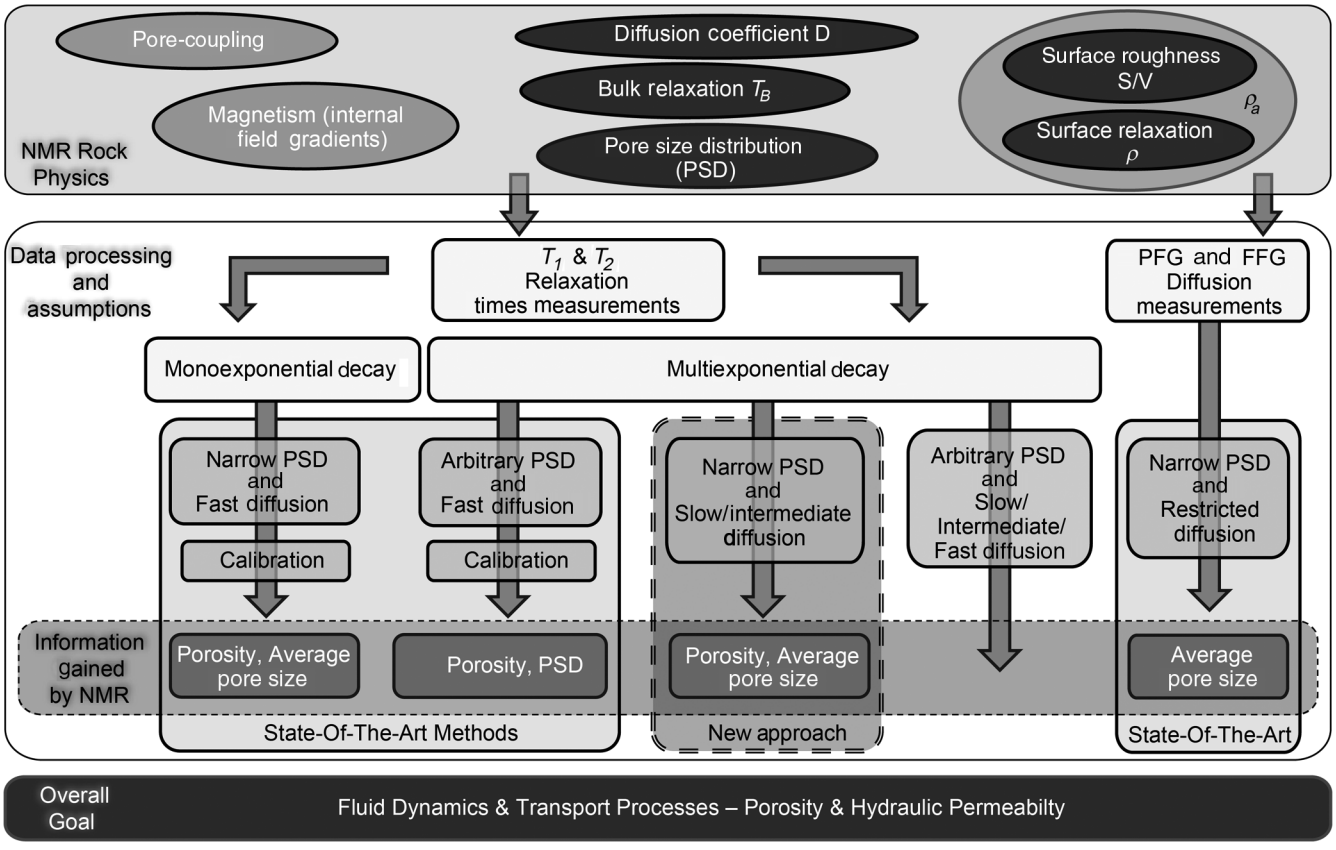

Figure 1. NMR relaxation and diffusion measurements (center) are used to deduce physical rock and fluid parameters (top). The T_1 and T_2 relaxation times are mono- or multiexponential. Different models are used to determine the porosity and PSD from the relaxation behavior, and they depend on the diffusion (fast, intermediate, slow) regime. Diffusion measurements may be applied in a PFG or FFG mode and rely on restricted-diffusion conditions. The overall goal is to provide the hydraulic properties of the subsurface from NMR during logging or from the earth's surface to investigate fluid flow and transport processes.

In this contribution, we hypothesize that average pore sizes can be estimated outside the fast-diffusion regime without the calibration of ρ. The method can be used for conventional relaxation time measurements that are available for in situ experimental techniques, such as for surface NMR and shallow groundwater NMR logging. Recent developments have shown that reliable relaxation-time measurements of T_1 or T_2 are feasible for surface NMR measurements (Grunewald and Walsh, 2013; Müller-Petke et al., 2013).

We develop a forward modeling code based on the equations given in Brownstein and Tarr (1979) and the following assumptions: (1) the surface relaxivity ρ is homogeneous and (2) the pore coupling and internal field gradients are negligible. Using this forward code, we examine the ability of inverse modeling to extract pore sizes without calibration from synthetic signals under the assumption of narrow PSDs and multiexponential decay due to only higher order modes. We evaluate whether pore sizes can be unambiguously estimated and what the corresponding uncertainties are. Numerical 2D finite-element simulations (Lehmann-Horn et al., 2007) are used to investigate the effect of an increasing inner surface (fractal rock-fluid interface) of single pores and to evaluate if surface roughness plays a key role in the departure from the fast-diffusion regime. Theoretical considerations are validated via laboratory experiments based on synthetic and natural unconsolidated materials with different pore sizes and surface relaxivities.

NMR RELAXATION TIMES THEORY

Torrey (1956) presents a governing diffusion equation to calculate the NMR relaxation time of a single water-saturated pore. Brownstein and Tarr (1979) express solutions to this governing equation for three simple geometries (planar, cylindrical, and spherical) as a sum of n "normal modes." These normal modes correspond to orthogonal spatial eigenfunctions that build the solution space to the diffusion equation transferred to an eigenvalue problem, with the inverse of the relaxation time being the eigenvalues. For cylindrical geometry, the solution reads

$$T_n = r_t^2/D\eta_n^2, \tag{1}$$

$$I_n = 4J_1^2(\eta_n)/\eta_n^2[J_0^2(\eta_n) + J_1^2(\eta_n)], \tag{2}$$

where T_n is the nth relaxation time, I_n is the relative intensity of the nth relaxation time, r_t is the radius of the cylinder, and $J_{0,1}$ are cylindrical Bessel functions of the zeroth and first order. The η_n terms are the positive roots of

$$\eta_n J_1(\eta_n)/J_0(\eta_n) = \rho r_t/D, \tag{3}$$

where D is the self-diffusion coefficient of the fluid and ρ is the material-specific surface relaxivity describing the interaction of the protons with the pore surface. Note that Brownstein and Tarr (1979) refer in their original paper to the longitudinal relaxation time T_1. Because the equations are valid for the longitudinal and transverse relaxation times T_2 by assigning an individual surface relaxivity $\rho_{1,2}$, we decided to skip any subindex for simplicity here and in the following.

Although Brownstein and Tarr (1979) neglect the relaxation time of the bulk fluid T_B, we extend equation 1 to

$$\frac{1}{T_n} = \frac{1}{T_B} + \frac{D\eta_n^2}{r_t^2}. \tag{4}$$

Incorporating T_B is necessary if relaxation due to the interaction of the protons with the pore surface is not significantly faster or even slower than the bulk relaxation time. In particular, this is the case for materials containing large pores (e.g., Dlugosch et al., 2013; Dlubac et al., 2014) that are of interest for this study.

One major outcome of the work of Brownstein and Tarr (1979) is summarized in Figure 2. Depending on the value of the term $\kappa = \rho r_t/D$, three regimes are distinguished:

- Fast-diffusion regime: The NMR signals are approximately monoexponential; i.e., the intensity of the zeroth mode is close to one and all the other intensities are negligible. Brownstein and Tarr (1979) give $\kappa \ll 1$ as a criterion for fast diffusion, whereas Ryu (2009) more explicitly gives $\kappa \leq 0.1$.

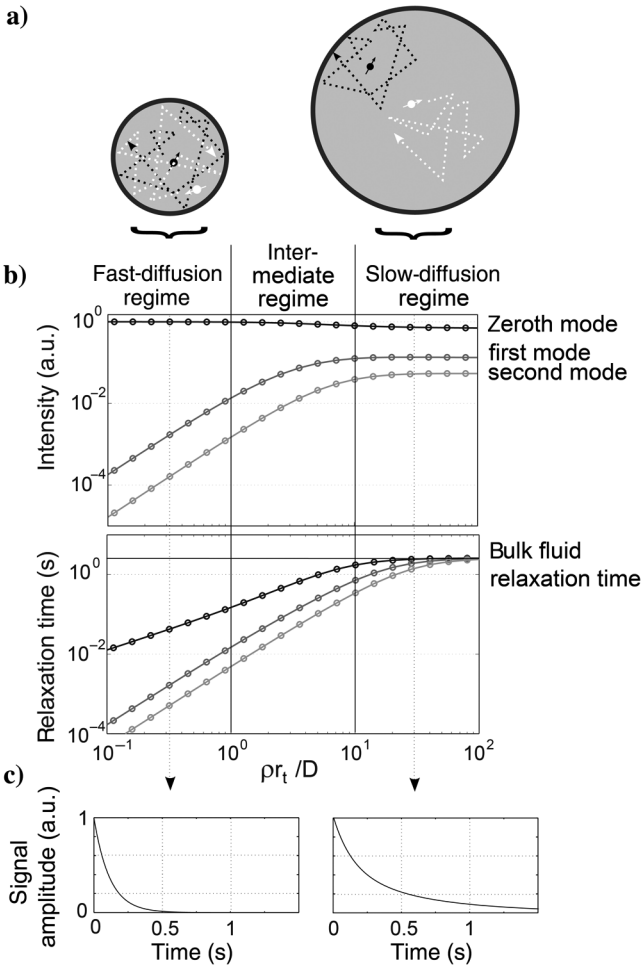

Figure 2. NMR forward response according to Brownstein and Tarr (1979) for cylindrical pores. The signal intensity and relaxation times for the zeroth to second mode as a function of the tube radius r_t, surface relaxivity ρ, self-diffusion D, and bulk relaxation time are shown in panel (b). The sketches in panels (a and c) for small and large tubes qualitatively show the pathways of two hydrogen protons during relaxation (a) and the resulting time-dependent decay as a superposition of the modes (c). The decay is monoexponential in the fast-diffusion regime (small pores), whereas the decay is multiexponential outside the fast-diffusion regime (larger pores).

- Intermediate-diffusion regime: The NMR signals are significantly multiexponential; i.e., the contributions of higher modes are nonnegligible, $1 \ll \kappa \ll 10$.
- Slow-diffusion regime: The NMR signals are still dominated by the zeroth mode, but the contributions of the higher modes sum up to a few tens of percent, $\kappa \gg 10$.

For this paper, we incorporate higher order modes into the data analyses. Because the intermediate and slow-diffusion regimes are assumed to show nonnegligible intensities for higher modes, we refer to those two cases as being "outside the fast-diffusion regime."

Fast-diffusion regime

In the fast-diffusion regime, the solution for the zeroth mode (the first root in the equation 3 and the main relaxation time) is (Brownstein and Tarr, 1979)

$$T_{n=0} = \frac{r_t}{\rho}. \tag{5}$$

Note that in equation 5, T_B has been neglected. The value T_B can be neglected if, as commonly assumed for fast diffusion (e.g., Dunn et al., 2002), T_B is smaller compared to r_t/ρ. Nevertheless, there are cases in which T_B needs to be considered (Dlubac et al., 2014). In any case, this relationship links the NMR relaxation time to pore size. If a multiexponential signal is measured and fast diffusion can be assumed, the RTD can be related to a PSD. However, the relationship needs to be calibrated because ρ is unknown and material specific.

Outside the fast-diffusion regime

Outside the fast-diffusion regime, RTDs cannot be easily linked to different pore sizes because multiexponential signals arise from a single pore volume. One extreme type of these conditions is slow diffusion ($\kappa \gg 10$). As discussed in Brownstein and Tarr (1979), the zeroth relaxation time becomes independent of ρ, and, neglecting T_B, the pore sizes can be directly measured.

If we account for T_B, the zeroth relaxation time may be close to T_B (Figure 2) and will therefore be difficult to use to estimate the pore size. A closer look at the first and second modes, however, reveals that the interpretation of these higher modes may also allow us to estimate the pore size. These modes are also affected by T_B, but to a lesser extent as shown in Figure 2 and equation 4, where $D\eta_n^2/r_t^2$ dominates $1/T_B$ with increasing n. Assuming ρ and D are constant, a change in r_t impacts the relaxation times and intensities of the higher modes. Thus, it appears attractive to evaluate whether pore-size information can be extracted from NMR by accounting for higher modes.

SIMULATION

Brownstein and Tarr cylindrical pore-space modeling

To evaluate whether higher modes can be used to interpret NMR measurements, a forward algorithm has been developed based on equations 1–4. This algorithm calculates an NMR signal for a given cylindrical tube radius r_t, surface relaxivity ρ, self-diffusion coefficient D, and bulk relaxation time T_B. We refer to a model that is used to calculate a signal based on the formulation of Brownstein and Tarr (1979) as a BT model.

For the synthetic study, one signal d_{obs} is calculated for two BT models with r_t of 80 and 500 μm, ρ of 10 μm/s and 100 μm/s, $D = 2.1\text{e}-9$ m^2/s, and $T_B = 3$ s. The signal is contaminated with 0.1% Gaussian noise; i.e., a random signal following the Gaussian distribution with a standard deviation of 0.001 is added to the data. This signal is then treated as the observed data. Next, the signals d_{est} are calculated by varying the material-specific parameters r_t and ρ while keeping the fluid parameters D and T_B constant. The residuals between d_{obs} and d_{est} display if other parameter sets of r_t and ρ generate similar data. We generate a map of the residuals over a certain parameter range for r_t and ρ to explore the correlations of the parameters. We use error-weighted residuals χ^2 to determine if a model is acceptable. A χ^2 of one indicates fitting the data within the noise. We prefer χ^2 because implementing appropriate error estimates is favorable for inversion (Günther et al., 2006).

Two BT models, the fast-diffusion regime (Figure 3a and 3c) and the intermediate/slow regime (Figure 3b and 3d), are chosen to distinguish the two fundamental cases. Because the data are contaminated with noise, both cases have several parameter combinations that fit the data within the noise level. This demonstrates the uncertainty associated with noise contamination.

The data set described approximately by the fast-diffusion regime ($\kappa = 0.38$) is monoexponential within the data error; i.e., the amplitudes of the higher modes are negligible. Consequently, any combination of r_t and ρ that satisfies equation 5 and the conditions of the fast-diffusion regime can explain the data set; i.e., r_t and ρ are strongly correlated (white dashed line in Figure 3). Only the maximum pore size can be obtained. Note that neglecting higher modes to derive equation 5 is not applicable for noise-free data.

The multiexponential data set that is described by the intermediate/slow regime ($\kappa = 23$) does not show this correlation between r_t and ρ. Because the data are contaminated with noise, there is some uncertainty associated with the solution, but there is no inherent correlation between the two parameters. A change in r_t cannot be compensated by a change in ρ. Therefore, the pore size could be obtained from the measured data (white cross in Figure 3).

At this point, we would like to emphasize that this method is based on fitting the decaying signal; i.e., we calculate the decaying signal for the parameters r_t, ρ, D, and T_B and compare these data with a measured decay. We do not fit the decaying signal to some finite number of relaxation times (biexponential, triexponential, ...) and analyze these extracted relaxation times as modes to find the corresponding parameter; such an approach would introduce additional uncertainty because two ill-posed problems (exponential fitting and fitting for higher modes) need to be solved instead of one.

Furthermore, we note that the presented approach of estimating r_t and ρ does not rely on a prior calculation of the diffusion regime. The BT modeling delivers r_t and ρ and their respective uncertainties. The obtained uncertainties can be used to distinguish the diffusion regimes because the correlation between r_t and ρ decreases when leaving the fast-diffusion regime.

Because we expect that the ability to infer the BT parameters from the measured data depends on the signal-to-noise ratio (S/N), we also carried out simulations for $r_t = 300$ μm, $\rho = 100$ μm/s, $D = 2.1\text{e}-9$ m^2/s, and $T_B = 3$ s (leading to $\kappa = 14$), where the S/Ns were 100 (typical laboratory conditions), 10

(achievable conditions for borehole measurements), and 1 (poor borehole conditions). We found (Figure 4) that S/Ns down to 10 for this parameter combination still allow for reasonable estimates of the pore size ($200 < r_t < 400$ μm) and surface relaxivity ($70 < \rho < 110$ μm/s), whereas the uncertainties rapidly increase for a lower S/N. This uncertainty analysis was carried out by parameter variation; i.e., a grid search was applied to find all combinations of r_t and ρ that satisfy the given data for the different S/Ns. The results are not that surprising because the total intensity of the higher modes sums to approximately 10% of the total signal intensity for this example. Nevertheless, the methodology can be used to estimate parameters even when the data quality is similar to that found in borehole measurements.

2D finite-element simulations accounting for rough rock-fluid interfaces

The analytical solutions given in Brownstein and Tarr (1979) are derived for smooth interfaces and simple geometries. To simulate the impact of rough interfaces similar to those present in rocks, we use a finite-element forward modeling (FEM) code to solve the diffusion equation in (Brownstein and Tarr, 1979) in 2D (Lehmann-Horn et al., 2007). We have simulated two cases: A (Figure 5a and 5b) and B (Figure 5d and 5e). Each shares the same surface relaxivity $\rho = 10$ μm/s and average pore size but differs in the roughness of the pore rock-fluid interface by a factor of three (see Table 1 for details). By comparing the simulations for the two cases (Figure 5), we found that increasing the interface roughness leads to shorter relaxation times. This confirms laboratory observations obtained from glass beads treated to increase their surface roughness (Keating, 2014). Apart from the impact on the mean relaxation time, case A (with the less rough interface, Figure 5b) shows a nearly monoexponential decay, whereas case B (with the rougher interface, Figure 5f) shows a multiexponential decay; i.e., the amplitudes of the higher-order modes are larger.

Next, we calculated the controlling parameter κ to determine the diffusion regime (Table 1). Analogous to the study of Keating and Falzone (2013), we distinguish two radii, an upper and lower radius. However, because the FEM simulations are 2D, our upper radius r_{max} is calculated from a circle with an equivalent area to the pore, whereas our lower radius r_{min} is calculated from the ratio of the circumference to the area. Using r_{max} obviously gives the same κ for both cases because the pore areas are similar. Using r_{min}, κ decreases for case B as r_{min} decreases. Consequently, both types of κ do not reflect the effect demonstrated by the simulation; the intensity of higher modes is larger for higher roughness.

For demonstration purposes, we apply the cylindrical (3D) BT inverse modeling scheme to the predicted NMR signals of our 2D fractal pore space. The synthetic decay signals are contaminated with 0.1% Gaussian noise. First, we found that the FEM response for both cases (A and B) can be sufficiently explained by smooth models derived from BT modeling (Figure 5c and 5f). Second, the FEM response for case A can be explained by several smooth models (dashed area in Figure 5c), in which the r_t and ρ for these models show a linear correlation as expected for fast-diffusion conditions.

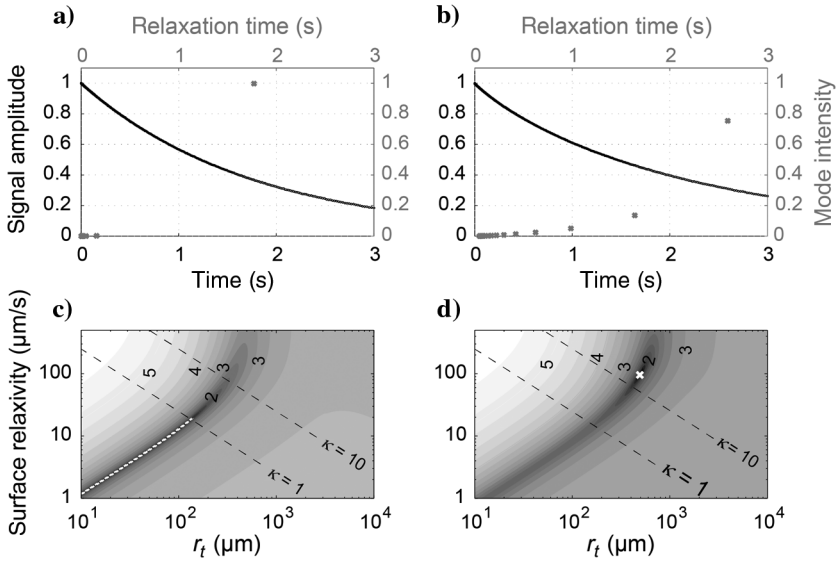

Figure 3. Brownstein and Tarr (1979) forward response for two different tube radii r_t (80 and 500 μm) and surface relaxivities ρ (10 μm/s and 100 μm/s) in panels (a and b), respectively. The modes' intensities and relaxation times are given as crosses, whereas the decaying signal is given as a solid line. The self-diffusion coefficient ($D = 2.1\text{e}-9$ m^2/s) and bulk relaxation time ($T_B = 3$ s) are the same in both cases. The data are contaminated with 0.1% Gaussian noise equivalent to a signal-to-noise ratio (S/N) of 1000. Panels (c and d) show the logarithm of the error-weighted residuals $\log_{10}(\chi^2)$ (black to white refers to low and high; the numbers refer to the contour line value) to the responses in panels (a and b) for variations in the surface relaxivity and tube radius. The black dashed lines indicate the slow- and fast-diffusion regimes. The white dashed line and the white cross indicate all parameter combinations of r_t and ρ that provide a data fit within the level of noise contamination ($\chi^2 = 1$).

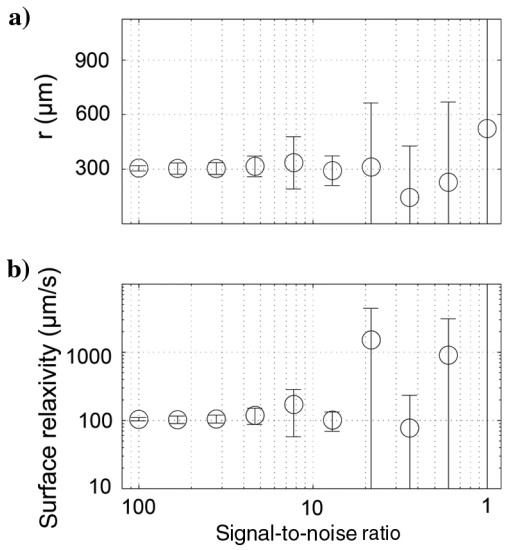

Figure 4. Parameter uncertainty for r_t (a) and ρ (b) as a function of the S/N. An S/N of 100 represents typical laboratory conditions, whereas an S/N of 10 is achievable for borehole measurements and 1 for poor borehole conditions.

BT modeling cannot be used to determine an average pore size. Third, the FEM response for case B can be explained by only a few smooth models (white cross in Figure 5f) as expected for a diffusion regime outside the fast-diffusion regime. BT modeling can be used to determine an average pore size that matches the pore size used for the FEM modeling, but the derived $\rho = 60$ μm/s is larger than the value used in the model by a factor of 6. Even though a full 3D finite-element simulation was used for quantitative interpretation, this example highlights that pore roughness controls the diffusion regime, which is in agreement with Sapoval et al. (1996). Moreover, as commented by Kenyon (1997), Ramakrishnan et al. (1998), and Kleinberg (1996), an apparent surface relaxivity ρ_a that is a function of the true, material-specific ρ, pore roughness, clay content, and nonsimple pore shapes controls the NMR relaxation time. Considering this ρ_a of 60 μm/s and the estimated pore radius of about 140 μm, we obtain $\kappa = 4$, which actually indicates diffusion outside the fast-diffusion regime and agrees with the observations of the simulated signals.

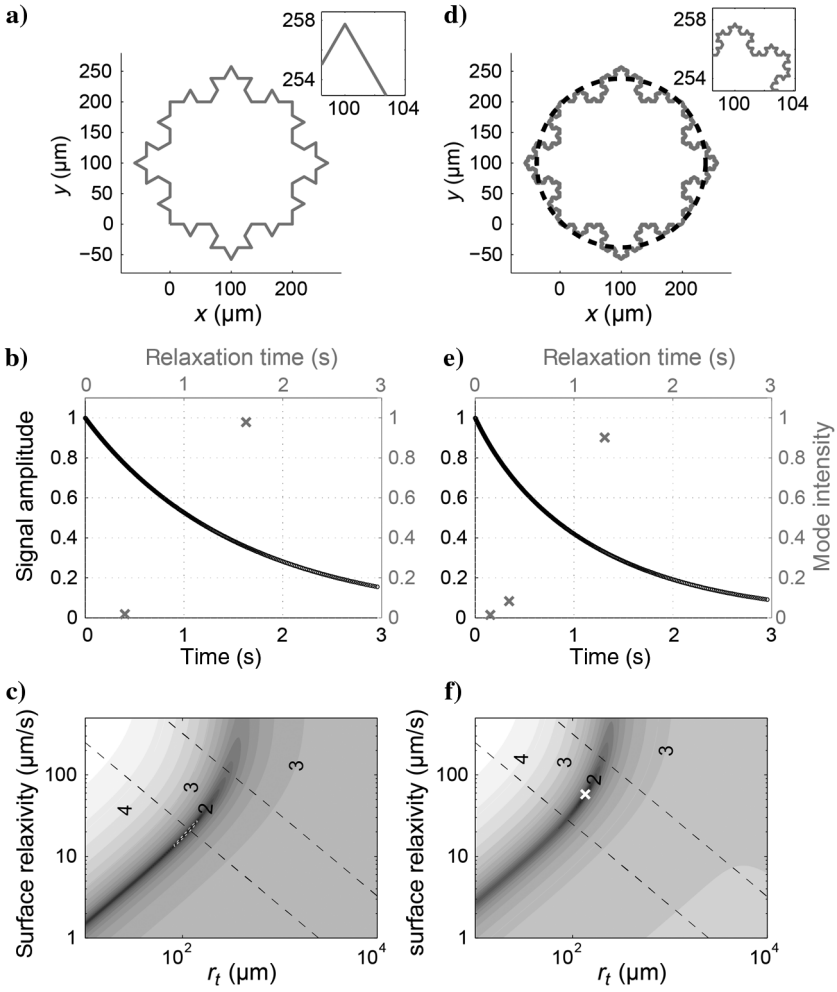

Figure 5. Two-dimensional finite-element forward response for two cases (panels a and d) with equal surface relaxivities ($\rho = 10$ μm/s), self-diffusion coefficients ($D = 2.1\text{e}-9$ m^2/s) and bulk relaxation times ($T_B = 3$ s) but increasing the inner surface by a factor of 3 in panel (d). In panels (b and e), the forward response is calculated using FEM; the crosses give the mode intensity and relaxation time, and the solid line is the decaying signal. Panels (c and f) show the logarithm of the error-weighted residual $\log_{10}(\chi^2)$ (black to white refers to low and high; the numbers refer to the contour line values) to the response of a BT model for variations in the surface relaxivity and tube radius. The black dashed lines indicate the slow- and fast-diffusion regimes. The white dashed line in panel (c) indicates all parameter combinations of r_t and ρ that provide a data fit within the level of data error ($\chi^2 = 1$). The white cross in panel (f) presents the best fitting model and corresponds to the black dashed circle in panel (d).

LABORATORY MEASUREMENTS

Sample selection, preparation, and characterization

Because BT forward modeling is based on a single pore size, we use samples from a very narrow PSD. We first choose glass beads to create well-defined samples over a range of grain sizes (d_{grain} between 90 m and 4.4 mm). The beads (Sigmund Lindner GmbH, Warmensteinach, Germany) consist of soda-lime glass with a chemical composition of mainly SiO_2, 54.7%; Al_2O_3, 14.5%; CaO, 22.5%; and B_2O_3, 5.5%. The particles are spherically shaped and split into samples with a narrow range of grain sizes as shown in Table 2. Secondly, sand samples with a high quartz content (Euroquarz GmbH, Dorsten, Germany) but natural grain shapes are used (Table 3).

In addition to selecting samples with different pore sizes, samples showing different surface relaxivities and, in the best case, equal pore sizes are worth considering. It has been shown that surface relaxivity is a function of the amount of iron oxides (Foley et al., 1996; Keating and Knight, 2007). Two options are available to experimentally alter the surface relaxivity. Keating and Knight (2007) realize this by conducting measurements on clean sand samples and sand coated with iron oxides. We select a natural sample originating from a drilling at the North Sea island of Borkum, Germany, from approximately 2 m deep. We refer to this sample as the B1 sample. B1 is treated using an ammonium oxalate process followed by a dithionite process to reduce the iron (III) oxides such as goethite, ferrihydrite, and maghemite to iron (II), which is aqueous under the chemical conditions present in this study. We use this procedure because it is the least destructive to silicates (Mehra and Jackson, 1960). We find an iron content of 500 mg/kg or 0.05% for the original sample. This iron content is not very unusual for natural samples. The iron content is visible from the reddish color of the sample (Figure 6), and it is apparent that there is less iron in the dithionite-treated sample due to the change in color. B1 consists of medium to fine sand. Therefore, we use this sample to first conduct measurements on the original state and then treat the material to dissolve the iron from the pore surfaces before measuring again. Even though the mass percent of iron used by Keating and Knight (2007) is significantly higher, this approach should enable us to conduct measurements on the same sample material for different surface relaxivities.

We use the effective grain diameter after Carrier (2003):

$$d_{\text{grain}} = 1/\sum \frac{f_i}{d_{li}^{0.5} d_{si}^{0.5}}, \quad (6)$$

where f_i is the (dimensionless) fraction of particles between the sieve sizes d_{li} and d_{si}, which are the respective sieve size limits. This effective grain diameter and the sample porosity Φ allow the average pore size of each sample to be calculated (e.g., Dlugosch et al., 2013):

$$a_{\text{sieve}} = \frac{1}{3}\frac{\Phi}{1-\Phi} d_{\text{grain}}. \quad (7)$$

Experimental setup

To visually check the packing of the material, we use a translucent polycarbonate sample holder with a length of 110 mm and an inner diameter of 40 mm. The dimension is chosen to be large enough to hold a representative volume of the material but still fit in the coil of the laboratory's NMR system. The samples are saturated with degassed and deionized water with sodium chloride to reach an electric conductivity of 400 µS/cm to minimize unwanted dissolution processes. The sample holder is first filled with fluid, and then the grains are slowly added to the water column to prevent air pockets. The material is gradually filled and compacted with a pestle to achieve similar porosities.

The NMR measurements are carried out using the Rock Core Analyzer (Magritek, Wellington, New Zealand), which operates at 2 MHz. We use a CPMG pulse sequence with an echo spacing of 200 µs. Because the diffusion relaxation rate T_D is neglected in equation 4, measurements at different echo spacings are carried out to confirm that this assumption is valid for our samples at an echo spacing of 200 µs. We use the built-in cooling/heating system to ensure a constant sample temperature between 21°C and 22°C during the measurements. Because T_B is not only a function of temperature and can be altered by dissolved ions, we estimate T_B separately for every sample. Therefore, after the NMR experiments on the sample, we extract the pore fluid and measured $T_{2,B}$ of the liquid. We find $T_{2,B} = 2.4 \pm 0.1$ s for all samples.

Pore size estimation for glass beads

Selecting two samples of different grain sizes, we present the results for the glass beads. First, the measured data d_{obs} (Figure 7a and 7d) are fit to the common multiexponential approach to derive a smooth RTD (Figure 7b and 7e). A regularization parameter λ is used to weigh the minimum structure in the RTD and minimum residual between the measured data and model response (see, e.g., Whittall et al., 1991). The data are preintegrated into 500 logarithmically spaced time bins. We allow for 300 logarithmically spaced relaxation time bins from 0.01 to 5 s during the inversion. We use an error-weighted inversion

Table 1. FEM modeling parameter: upper r_{max} and lower r_{min} radius describing a circle with an equivalent area of the pore or based on the ratio of the circumference to the area, respectively; the controlling parameter κ is typically used to obtain the diffusion regime.

	Case A	Case B
ρ_{true} (µm/s)	10	10
T_B (s)	3	3
Circumference c (µm)	1422	4495
Area a (µm^2)	51,119	53,750
$r_{\text{max}} = \sqrt{a/\pi}$ (µm)	127	130
$r_{\text{min}} = 2 \cdot a/c$ (µm)	71	23
$\kappa(\rho_{\text{true}}, r_{\text{min}})$	0.34	0.11
$\kappa(\rho_{\text{true}}, r_{\text{max}})$	0.6	0.6

Table 2. List of sample parameters as derived from the sieving and NMR analyses for the set of glass beads.

Material	$d_{\text{grain}}^{\text{sieving}}$ (µm)	Φ^{NMR}	$r_{\text{pore}}^{\text{sieving}}$ (µm)	$r_{\text{pore}}^{\text{NMR}}$ (µm)	ρ (µm/s)
Glass beads	4400–3600	0.39	930–760	630–710	330–170
	1650–1250	0.35	300–225	350–250	110–85
	500–250	0.38	100–50	110–90	140–100
	125–100	0.37	23–18	<30	<270

Table 3. List of sample parameters as derived from the sieving and NMR analyses for the natural sand samples.

Material	$d_{\text{grain}}^{\text{sieving}}$ (µm)	Φ^{NMR}	$r_{\text{pore}}^{\text{sieving}}$ (µm)	$r_{\text{pore}}^{\text{NMR}}$ (µm)	ρ (µm/s)
Quartz sand	2000–630	0.41	450–150	400–300	300–150
	1000–500	0.38	200–100	170–155	320–250
	500–125	0.34	85–21	80–72	170–120

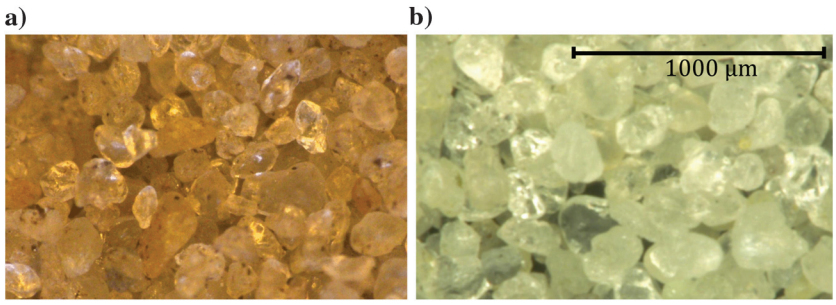

Figure 6. Microphotography of the B1 samples (a) before and (b) after chemical treatment to dissolve free iron.

scheme (Günther et al., 2006) to account for the logarithmic data preintegration that changes the error for each time bin. Using this approach, the data are fit within the acceptable level of data error (to avoid overfitting), and no structure remains in the error-weighted residuals that would indicate unexplained data. Therefore, the residuals for the RTD display a benchmark for the BT modeling. Second, similar to the synthetic study, the BT model parameter space of r_t and ρ is varied to calculate the estimated data d_{est}, and the residuals between each d_{est} and the measured data are calculated (Figure 7c and 7f). The best-fitting BT models are indicated by the area framed by a white dashed line. All the models within this area satisfy the measured data as well as the RTD (detailed residuals for each of the BT models are given for comparison in Figure 7a and 7d). The two samples represent the two cases as discussed for the synthetic examples: a first case with small grain sizes that does not show a distinct minimum and therefore shows a strong correlation with r_t and ρ and a second case that shows a distinct minimum and allows the pore radius to be directly estimated. For a comparison to the T_2 distribution, the higher order modes are given in Figure 7b and 7e. Note that we scaled the amplitudes of the RTD such that the maximum of the RTD matches the amplitude of the zeroth mode. Without scaling, the amplitudes of all the relaxation time bins for the RTD and the amplitudes of all the modes sum up to the same total water content of the sample. Thus, the amplitudes of the RTD are necessarily far below the modes. To ease the comparison, we prefer to scale the RTD. For a comparison of the RTD and the modes, one should keep in mind this scaling and the fact that each mode amplitude reflects a certain area of the RTD. Thus, the amplitudes and relaxation times of the modes nicely match the distribution. The relaxation time of the zeroth mode and the maximum of the RTD are very close in both cases. Concerning the second case (Figure 7e), the left-side tail of the RTD is represented by the higher order modes. However, the most important observation for the second diffusion case outside the fast-diffusion scheme is an average pore size of 350–250 μm, which is well within the estimated pore size of 310–270 μm derived from the grain sizes from the sieving analyses (Table 2). In addition to the pore size, we obtain ρ within the interval of $110 - 85$ μm/s. Table 2 summarizes the results for all samples, showing the grain size, porosity, pore size derived from sieving, pore size derived from NMR, and the corresponding surface relaxivity ρ. All measured data can be explained by the BT modeling within the level of noise and is therefore similar to the data fit obtained from a standard T_2 distribution. Overall, a good agreement between the pore sizes obtained from NMR and from the grain sizes is achieved.

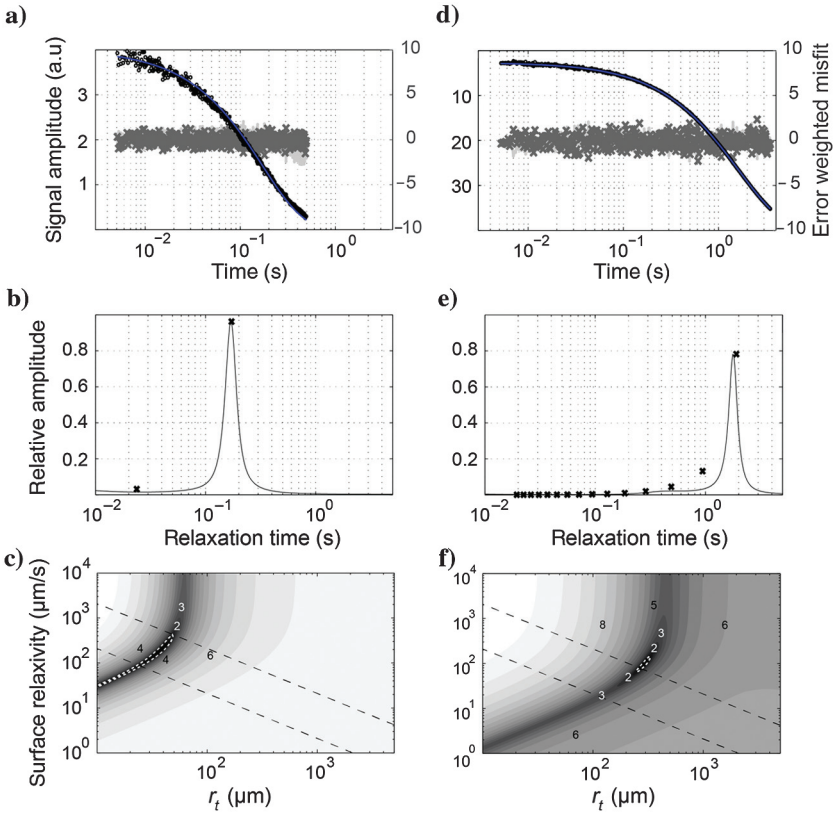

Figure 7. RTDs and BT modeling for two samples of glass beads with grain sizes ranging (a-c) from 125 to 100 μm and (d-f) from 1650 μm to 1250 μm. The measured data (black), residuals of the forward response from the best fitting BT modeling (light gray), and T_2 distribution (gray) for the measured data in terms of the error weighted misfit are shown in panels (a and d). The BT model (black crosses) and T_2 distribution (solid line) are presented in panels (b and e). Panels (c and f) show the logarithm of the error weighted residuals for different BT models. The black dashed lines indicate the slow- and fast-diffusion regions. The white dashed line indicates all parameter combinations of r_t and ρ that provide a data fit within the level of the data error.

Pore size estimation for natural sand

Figure 8 illustrates the detailed results for one sample of natural sand, and the results for all measured samples are summarized in Table 3. The residuals between the measured data and each BT model (Figure 8c) have a significant minimum. The residuals (light gray in Figure 8a) for the best fitting BT models (indicated by the area framed by a white dashed line in Figure 8c) do not show any remaining structure, indicating an acceptable data fit. The deviations (dark gray) in a standard T_2-distribution are within the same range. Thus, BT modeling for this natural sand sample is able to sufficiently explain the measured data within the measurement error and equally well compared to an RTD. The average pore sizes, which are as important as the data fit, are again well within the results of the sieving analyses (Table 3), enabling BT modeling to predict pore sizes from NMR measurements without any calibration.

Reliability of pore-size estimations

We select the measurements of the B1 sample to evaluate the reliability of the pore-size estimation procedure and to test whether multiexponential decays are due to the diffusion conditions or to the PSDs. The measured data (Figure 9a) of the original sample are significantly multiexponential, and the distribution shows a tail at shorter times. The measured data (Figure 9d) after treatment clearly show the impact of the change in ρ caused by the changing content of paramagnetic iron. The decay of the obtained

data is significantly slower compared with that of the original sample. The T_2 distribution looks remarkably different. The tail of short relaxation times has disappeared. However, the sample has not been significantly changed despite the dissolution process. Therefore, the change in the data is due to an increase in higher order modes.

The BT modeling nicely reflects that the pore size did not change; rather, ρ changed due to the dissolution process. The pore sizes estimated from the data of the two samples are approximately 50 and 70 μm, respectively, and are well within the results from the grain size analyses (Table 4). However, one would give significantly different PSDs for each sample based on the RTDs, especially in terms of the amount of fine grains. Moreover, as expected due to the decrease in paramagnetic content on the pore surface, the best fitting BT models estimate ρ to be 600 μm/s for the original sample and 120 μm/s after the sample is treated. The treated sample is close to fast-diffusion conditions as expected from the grain size and following a treatment that decreases surface relaxivity. We are, in fact, surprised to be still able to extract some information even though the uncertainties increased. Note that the data fit for the original sample is not as perfect as for all other samples. We think that this is most likely caused by a nonuniform distribution of surface relaxivity.

DISCUSSION

Pore roughness, apparent surface relaxivities, and diffusion regime

We show that average pore sizes can be obtained directly from NMR data using a BT modeling approach if relaxation occurs outside the fast-diffusion regime. In addition to r_t, ρ controls the diffusion regime, but the values of ρ observed for the data presented are unusually high, implying a slow- or intermediate-diffusion regime for pores typically assumed to be in the fast-diffusion regime. Consequently, we discuss these high surface relaxivities below.

Because ρ is an NMR intrinsic parameter, neither independent nor direct measurement techniques that can determine the value of ρ are available. Common procedures that determine ρ are based on the NMR measurement itself. Measuring the surface-area-to-pore-volume ratio (S/V) using, for instance, BET and assuming fast diffusion, ρ is calculated from the relaxation time using (Foley et al., 1996)

$$\frac{1}{T} = \rho \frac{S}{V}. \tag{8}$$

If the pore surface is smooth and of simple geometry, S/V can be transferred to a mean pore size, and the diffusion case can be calculated using the cases presented by Brownstein and Tarr (1979). However, if rough pore surfaces are present, ρ can be calculated using equation 8 to give the value for the surface relaxivity; however, according to the fractal surfaces implemented by our simulations, the diffusion case cannot be calculated by means of ρ and a mean pore size. In fact, it is necessary to account for pore roughness. We show preliminary attempts to explain the simulated data using smooth surfaces, an average pore size and a higher apparent surface relaxivity. Following this, the given surface relaxivities in this paper are the apparent surface relaxivities ρ_a and cannot be directly compared with the ρ derived from the S/V because the former are obtained from a method sensitive to pore roughness. A very simple example based on the results published by Keating and Knight (2010) appears illustrative. Using the S/V for a sample of quartz grains, the authors derive a pore radius of approximately 2 μm from BET measurements; based on a grain radius of 200 μm, simple cubic packing leads to a pore radius of approximately 150 μm. Thus, compared to a smooth surface, the real pore surface is increased by a factor of 75. This factor may explain the differences in ρ given in their paper and those written here.

The factor of 75 appears high but not impossible following the research on pore roughness published by Stallmach et al. (2002) and Pape et al. (2006). They give pore roughness in terms of the fractal dimension and report values ranging from 2.26 to 2.46 for sandstones and 2.2 for glacial sand deposits. Using the fractal dimension, a ratio between the BET-measured surface-area S_{BET} and the smooth surface obtained from the grain analyses or flow experiments S_{grain} is calculated as (Pape et al., 1999, 2006)

$$\frac{S_{\mathrm{BET}}}{S_{\mathrm{grain}}} = \left(\frac{\lambda_{\mathrm{BET}}}{\lambda_{\mathrm{grain}}}\right)^{2-D_{\mathrm{frac}}}, \tag{9}$$

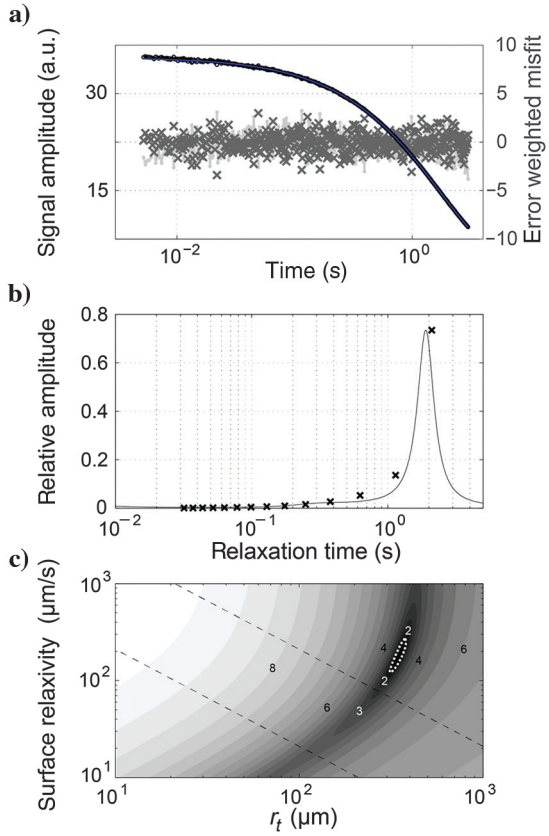

Figure 8. RTDs and BT modeling for a sample consisting of natural sand with grain sizes ranging from 2000 to 630 μm. The measured data (black), residuals of the forward response from the best fitting BT modeling (light gray) and T_2 distribution (gray) for the measured data in terms of the error weighted misfit are shown in panel (a). The BT model (black crosses) and T_2 distribution (solid line) are presented in panel (b). Panel (c) shows the logarithm of the error-weighted residuals for different BT models. The black dashed lines indicate the slow- and fast-diffusion regimes. The white dashed line indicates all parameter combinations of r_t and M that provide a data fit within the level of the data error.

where λ_{BET} is the minimum length resolved by the BET ($3 \cdot 10^{-10}$ m); λ_{grain} is the minimum (pore) length from the grain analyses, i.e., the minimal pore size; and D_{frac} is the fractal dimension. Considering $\lambda_{grain} = 150$ µm as above, D_{frac} would need to be 2.33 to obtain a factor of 75, whereas assuming D_{frac} to be 2.2 results in a factor of 14. Our numerical example shows an impact of pore roughness on the relaxation time and diffusion regime by a factor of 3. This emphasizes the need to develop appropriate equations that include pore roughness (or fractal dimension) when calculating the diffusion regime.

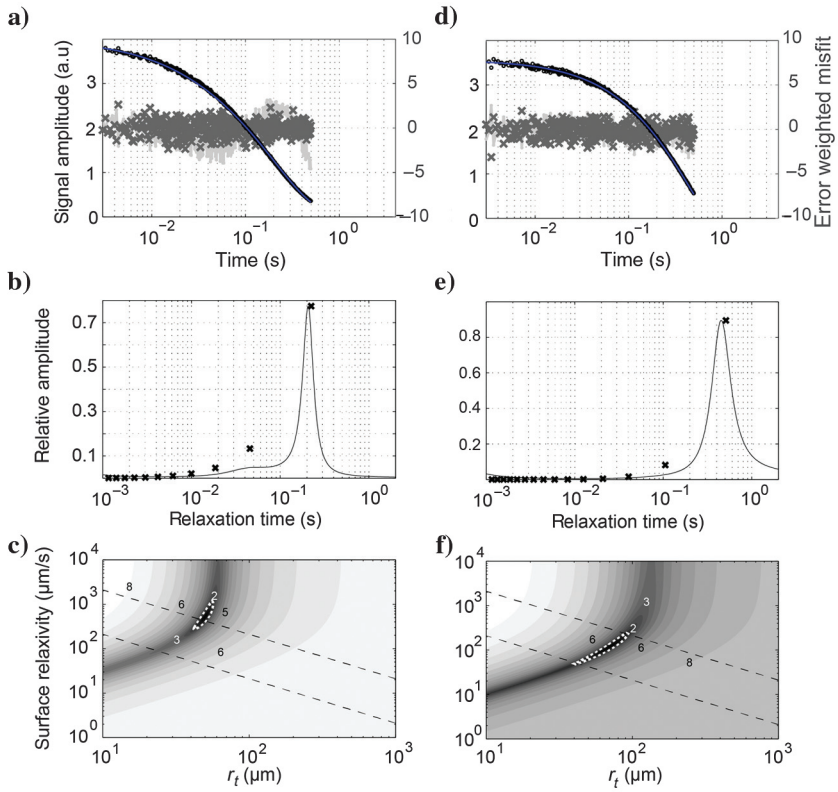

Figure 9. RTDs and BT modeling for the B1 sample (a-c) before and (d-e) after dissolving free iron. The measured data (black), residuals of the forward response from the best fitting BT modeling (light gray), and T_2 distribution (gray) for the measured data in terms of the error weighted misfit are shown in panels (a and d). The BT model (black crosses) and T_2 distribution (solid line) are presented in panels (b and e). Panels (c and f) show the logarithm of the error-weighted residuals for different BT models. The black dashed lines indicate the slow- and fast-diffusion regimes. The white dashed line indicates all parameter combinations of r_t and ρ that provide a data fit within the level of the data error.

Table 4. List of sample parameters as derived from the sieving and NMR analyses for the B1 sample.

Material	$d_{grain}^{sieving}$ (µm)	Φ^{NMR}	$r_{pore}^{sieving}$ (µm)	r_{pore}^{NMR} (µm)	ρ (µm/s)
B1 original	300–100	0.41	70–23	60–45	1000–150
B1 treated	300–100	0.39	63–21	100–40	200–50

Multiexponential decays, nonuniform surface relaxivities, and narrow PSDs

In addition to high (apparent) surface relaxivities, we expect a dispute arising from the ambiguity of multiexponential relaxation caused by the PSD, higher order modes, or inhomogeneous distribution of surface relaxivity. We show multiexponential signals caused by higher order modes. However, in many cases, the multiexponential signals are due to broad PSDs. We limited this study to samples of small grain size distributions to avoid this ambiguity. In practice, this reflects the need of strong a priori knowledge and shows that one should look at the error connected with assuming the wrong case. Moreover, what happens in the most general case (see Figure 1) of a sample that exhibits relaxation in larger pores outside the fast diffusion regime and smaller pores within the fast-diffusion regime?

We controlled the PSDs by selecting appropriate samples with narrow PSDs. Alternatively, we had no control on the distribution of surface relaxivity. Multiexponential relaxation may also be due to nonuniform distributions of surface relaxivities in the pore space. Following Keating and Falzone (2013), ρ is assumed to be homogeneous as long as the distance between two paramagnetic sites l_r is small relative to the distance that a proton can travel within the time scale of an NMR measurement l_D. They calculated l_D using $\sqrt{6DT}$, where T is the bulk relaxation time. For the samples presented in this study, l_D is approximately 180 µm. Consequently, for samples consisting of pores that are smaller than 180 µm, multiexponential relaxation should not be caused by nonuniform ρ distributions.

Nevertheless, multiexponential data caused by a nonuniform ρ distribution may be present for samples consisting of pores that are larger than 180 µm. However, we are able to explain these samples by higher modes using reasonable pore sizes. We argue that it is unlikely that the nonuniformity of ρ would be exactly such as to generate relaxation times matching those of the higher modes. The different values of ρ would have to be distributed in the pore space such that the relaxation times and amplitudes match the higher modes. Nevertheless, this is only an indication and no rigorous proof, but further investigation is beyond the scope of this paper. Therefore, we emphasize that research on this topic is necessary. One may extend the numerical simulations presented here by assigning different values of ρ to the boundaries and implementing multiple pores and pore throats connecting these pores. This numerical approach would also allow us to investigate the pore coupling assumption made in this study. One may also continue the laboratory study of Keating and Knight (2012) on the spatial variability of ρ and pore coupling by applying our methodology to these types of prepared samples. We recommend that this study

be treated as a starting point with significant limitations but high potential for further improvements.

CONCLUSIONS

We present an approach to estimate the average pore size for coarse-grained unconsolidated material by means of incorporating higher order modes in NMR decay time interpretation. This is relevant for in situ NMR experiments such as surface NMR or shallow NMR logging, in which PFG or FFG sequences are unavailable and one operates outside the fast-diffusion regime. A forward modeling study was carried out to show that the pore size can be obtained from measured relaxation times without calibration outside the fast-diffusion regime. A 2D finite-element fractal pore-space modeling example demonstrates that an apparent increase in the surface relaxivity can be observed when the roughness of the rock-fluid interface is increased. We found that pore roughness has a significant impact on the relaxation time and the diffusion regime. In agreement with others, we refer to an apparent surface relaxivity when surface roughness is neglected in the model. Measurements of glass bead and natural sand samples encompassing a small spectrum of grain sizes confirm that the presented approach can be applied to natural unconsolidated material. In addition to providing estimates of the pore sizes, measurements of a sample before and after it was treated to dissolve iron show that this approach can be used to estimate the surface relaxivity. The methodology is limited to material with a narrow PSD and a uniform distribution of ρ because we assume that the multiexponential decay is due only to higher order modes and not to an arbitrary PSD or nonuniform ρ distribution.

ACKNOWLEDGMENTS

We would like to thank K. Keating, two anonymous reviewers, and the associate editor for their comments, which helped to improve the clarity of the manuscript.

REFERENCES

Brakel, J. V., S. Modrý, and M. Svatá, 1981, Mercury porosimetry: State of the art: Powder Technology, **29**, 1–12, doi: 10.1016/0032-5910(81)85001-2.

Brooks, R. H., and A. T. Corey, 1964, Hydraulic properties of porous media: Hydrology papers: Colorado State University.

Brownstein, K. R., and C. E. Tarr, 1979, Importance of classical diffusion in NMR studies of water in biological cells: Physical Review A, **19**, 2446–2453, doi: 10.1103/PhysRevA.19.2446.

Butler, J. J., 2005, Hydrogeological methods for estimation of spatial variations in hydraulic conductivity, *in* Y. Rubin, and S. S. Hubbard, eds., Hydrogeophysics: Springer, vol. 50, Water Science and Technology Library, 23–58.

Callaghan, P. T., 2007, Principles of nuclear magnetic resonance microscopy: Oxford University Press.

Carman, P. C., 1939, Permeability of saturated sands, soils and clays: The Journal of Agricultural Science, **29**, 262–273, doi: 10.1017/S0021859600051789.

Carrier, W. D., 2003, Goodbye, Hazen; hello, Kozeny-Carman: Journal of Geotechnical and Geoenvironmental Engineering, **129**, 1054–1056, doi: 10.1061/(ASCE)1090-0241(2003)129:11(1054).

Coates, G. R., L. Xiao, and M. G. Prammer, 1999, NMR logging principles and application: Halliburton Energy Services.

Dlubac, K., R. Knight, and K. Keating, 2014, A numerical study of the relationship between NMR relaxation and permeability in sands and gravels: Near Surface Geophysics, **12**, 219–230, doi: 10.3997/1873-0604.2013042.

Dlubac, K., R. Knight, Y.-Q. Song, N. Bachman, B. Grau, J. Cannia, and J. Williams, 2013, Use of NMR logging to obtain estimates of hydraulic conductivity in the High Plains aquifer, Nebraska, USA: Water Resources Research, **49**, 1871–1886, doi: 10.1002/wrcr.20151.

Dlugosch, R., T. Günther, M. Müller-Petke, and U. Yaramanci, 2013, Improved prediction of hydraulic conductivity for coarse-grained, unconsolidated material from nuclear magnetic resonance: Geophysics, **78**, no. 4, EN55–EN64, doi: 10.1190/geo2012-0187.1.

Dlugosch, R., M. Mueller-Petke, T. Guenther, S. Costabel, and U. Yaramanci, 2011, Assessment of the potential of a new generation of surface NMR instruments: Near Surface Geophysics, **9**, 89–102, doi: 10.3997/1873-0604.2010063.

Dunn, K. J., D. J. Bergman, and G. A. Latorraca, 2002, Nuclear magnetic resonance, petrophysical and logging applications, 1st ed.: Pergamon.

Foley, I., S. A. Farooqui, and R. L. Kleinberg, 1996, Effect of paramagnetic ions on NMR relaxation of fluids at solid surfaces: Journal of Magnetic Resonance, Series A, **123**, 95–104, doi: 10.1006/jmra.1996.0218.

Fukushima, E., and S. B. W. Roeder, 1981, Experimental pulse NMR — A nuts and bolts approach: Westview Press.

Grunewald, E., and D. Walsh, 2013, Multiecho scheme advances surface NMR for aquifer characterization: Geophysical Research Letters, **40**, 6346–6350, doi: 10.1002/2013GL057607.

Günther, T., C. Rücker, and K. Spitzer, 2006, Three-dimensional modeling and inversion of DC resistivity data incorporating topography — Part II: Inversion: Geophysical Journal International, **166**, 506–517, doi: 10.1111/j.1365-246X.2006.03011.x.

Hürlimann, M. D., and D. D. Griffin, 2000, Spin dynamics of Carr-Purcell-Meiboom-Gill-like sequences in grossly inhomogeneous B0 and B1 fields and application to NMR well logging: Journal of Magnetic Resonance, **143**, 120–135, doi: 10.1006/jmre.1999.1967.

Hürlimann, M. D., K. G. Helmer, L. L. Latour, and C. H. Sotak, 1994, Restricted diffusion in sedimentary rocks. Determination of surface-area-to-volume ratio and surface relaxivity: Journal of Magnetic Resonance, Series A, **111**, 169–178, doi: 10.1006/jmra.1994.1243.

Hürlimann, M. D., and L. Venkataramanan, 2002, Quantitative measurement of two-dimensional distribution functions of diffusion and relaxation in grossly inhomogeneous fields: Journal of Magnetic Resonance, **157**, 31–42, doi: 10.1006/jmre.2002.2567.

Hürlimann, M. D., L. Venkataramanan, C. Flaum, P. Speier, C. Karmonik, R. Freedman, and N. Heaton, 2002, Diffusion-editing: New NMR measurement of saturation and pore geometry: Presented at SPWLA 43rd Annual Logging Symposium.

Keating, K., 2014, A laboratory study to determine the effect of surface area and bead diameter on NMR relaxation rates of glass bead packs: Near Surface Geophysics, **12**, 243–254, doi: 10.3997/1873-0604.2013064.

Keating, K., and S. Falzone, 2013, Relating nuclear magnetic resonance relaxation time distributions to void-size distributions for unconsolidated sand packs: Geophysics, **78**, no. 6, D461–D472, doi: 10.1190/geo2012-0461.1.

Keating, K., and R. Knight, 2007, A laboratory study to determine the effect of iron oxides on proton NMR measurements: Geophysics, **72**, no. 1, E27–E32, doi: 10.1190/1.2399445.

Keating, K., and R. Knight, 2010, A laboratory study of the effect of Fe (II)-bearing minerals on nuclear magnetic resonance (NMR) relaxation measurements: Geophysics, **75**, no. 3, F71–F82, doi: 10.1190/1.3386573.

Keating, K., and R. Knight, 2012, The effect of spatial variation in surface relaxivity on nuclear magnetic resonance relaxation rates: Geophysics, **77**, no. 5, E365–E377, doi: 10.1190/geo2011-0462.1.

Kenyon, W. E., 1997, Petrophysical principles of applications of NMR logging: The Log Analyst, **38**, 21–43.

Kenyon, W. E., P. I. Day, C. Straley, and J. F. Willemsen, 1988, A three-part study of NMR longitudinal relaxation properties of water-saturated sandstones: SPE Formation Evaluation, **3**, 622–636, doi: 10.2118/15643-PA.

Kleinberg, R., 1996, Utility of NMR T2 distributions, connection with capillary pressure, clay effect, and determination of the surface relaxivity parameter ρ_2: Magnetic Resonance Imaging, **14**, 761–767, doi: 10.1016/S0730-725X(96)00161-0.

Kozeny, J., 1927, Über kapillare Leitung des Wassers im Boden: Sitzungsberichte / Akademie der Wissenschaften in Wien, Mathematisch-Naturwissen-schaftliche Klasse Abteilung IIa, **136**, 271–306.

Lehmann-Horn, J., S. Strehl, and U. Yaramanci, 2007, Numerical simulations of NMR responses in fractal pore-space with the finite element method: Presented at Near Surface 2007 — 13th European Meeting of Environmental and Engineering Geophysics.

Mehra, O., and M. Jackson, 1960, Iron oxide removal from soils and clays by a dithionite-citrate system buffered with sodium bicarbonate: Clays and Clay Minerals, **7**, 317–327, 10.1346/CCMN.1958.0070122.

Mitra, P. P., P. N. Sen, and L. M. Schwartz, 1993, Short-time behavior of the diffusion coefficient as a geometrical probe of porous media: Physical Review B, **47**, 8565–8574, doi: 10.1103/PhysRevB.47.8565.

Müller-Petke, M., J. O. Walbrecker, and R. J. Knight, 2013, The inversion of surface-NMR T1 data for improved aquifer characterization: Geophysics, **78**, no. 6, EN83–EN94, doi: 10.1190/geo2013-0035.1.

Pape, H., C. Clauser, and J. Iffland, 1999, Permeability prediction based on fractal pore-space geometry: Geophysics, **64**, 1447–1460, doi: 10.1190/1.1444649.

Pape, H., J. E. Tillich, and M. Holz, 2006, Pore geometry of sandstone derived from pulsed field gradient NMR: Journal of Applied Geophysics, **58**, 232–252, doi: 10.1016/j.jappgeo.2005.07.002.

Parsekian, A., K. Dlubac, E. Grunewald, J. Butler, R. Knight, and D. Walsh, 2014, Bootstrap calibration and uncertainty estimation of downhole NMR hydraulic conductivity estimates in an unconsolidated aquifer: Ground Water, **53**, 111–121, doi: 10.1111/gwat.12165.

Ramakrishnan, T. S., L. M. Schwartz, E. J. Fordham, W. E. Kenyon, and D. J. Wilkinson, 1998, Forward models for nuclear magnetic resonance in carbonate rocks: Presented at SPWLA 39th Annual Logging Symposium.

Ryu, S., 2009, Effect of inhomogeneous surface relaxivity, pore geometry and internal field gradients on NMR logging: Exact and perturbative theories and numerical investigations: Presented at SPWLA 50th Annual Logging Symposium.

Sapoval, B., S. Russ, D. Petit, and J. P. Korb, 1996, Fractal geometry impact on nuclear relaxation in irregular pores: Magnetic Resonance Imaging, **14**, 863–867, doi: 10.1016/S0730-725X(96)00217-2.

Stallmach, F., and J. Kärger, 1999, The potentials of pulsed field gradient NMR for investigation of porous media: Adsorption, **5**, 117–133, doi: 10.1023/A:1008949607093.

Stallmach, F., C. Vogt, J. Kärger, K. Helbig, and F. Jacobs, 2002, Fractal geometry of surface areas of sand grains probed by pulsed field gradient NMR: Physical Review Letters, **88**, 105505, doi: 10.1103/PhysRevLett.88.105505.

Stejskal, E. O., and J. E. Tanner, 1965, Spin diffusion measurements: Spin echoes in the presence of a time-dependent field gradient: Journal of Chemical Physics, **42**, 288, doi: 10.1063/1.1695690.

Straley, C., A. Matteson, S. Feng, L. M. Schwartz, W. E. Kenyon, and J. R. Banavar, 1987, Magnetic resonance, digital image analysis, and permeability of porous media: Applied Physics Letters, **51**, 1146–1148, doi: 10.1063/1.98766.

Torrey, H. C., 1956, Bloch equations with diffusion terms: Physical Review, **104**, 563–565, doi: 10.1103/PhysRev.104.563.

Vogt, C., P. Galvosas, N. Klitzsch, and F. Stallmach, 2002, Self-diffusion studies of pore fluids in unconsolidated sediments by PFG NMR: Journal of Applied Geophysics, **50**, 455–467, doi: 10.1016/S0926-9851(02)00195-7.

Whittall, K. P., M. J. Bronskill, and R. M. Henkelman, 1991, Investigation of analysis techniques for complicated NMR relaxation data: Journal of Magnetic Resonance, **95**, 221–234, doi: 10.1016/0022-2364(91)90213-D.